Am J Transl Res 2023;15(11):6362-6380
www.ajtr.org /ISSN:1943-8141/AJTR0152816

Original Article

Yigan Mingmu Decoction inhibits diabetic macular edema through regulating Kir4.1/AQP4 axis: a study based on network pharmacology

Longrong Huang, Xinyi Guo, Qi Hu, Zhuoyu Hu, Peijuan Wu, Jian Jiang, Jing Liu, Zhimin Liu, Xiangdong Chen

Department of Ophthalmology, The First Affiliated Hospital of Hunan University of Chinese Medicine, Changsha 431000, Hunan, China

Received August 8, 2023; Accepted October 14, 2023; Epub November 15, 2023; Published November 30, 2023

Abstract: Objective: To explore the role and mechanism of Yigan Mingmu Decoction (YGMMD) in preventing and treating diabetic macular edema (DME). Methods: The bioactive compounds in YGMMD and their targets were screened using network pharmacology. Sprague Dawley (SD) rats were treated with the respective drugs: andomine, YGMMD-L, YGMMD-M, YGMMD-H for four weeks. Blood glucose, body weight, and morphologic indicators were measured, and hematoxylin and eosin (H&E) staining was used to assess retinal pathologic changes. Western blotting was used to monitor the expression of the phosphatidylinositol 3 kinase-protein kinase B (PI3K-AKT), pathway-related proteins aquaporin 4 (AQP4), inwardly rectifying potassium channel subtype 4.1 (Kir4.1), and phosphorylase extracellular regulated protein kinases (p-ERK1/2). Immunofluorescence was used to observe the expression levels of AQP4 and Kir4.1. Immunohistochemistry was performed to determine the expression of p-ERK1/2. Results: Pharmacologic network analysis and molecular docking suggested that YGMMD treatment of DME regulates AQP4/Kir4.1. *In vivo* experiments showed that YGMMD had significant hypoglycemic effects and reduced retinal edema in Sprague Dawley (SD) rats: YGMMD-H downregulated AQP4 and p-ERK1/2 and upregulated p-AKT and Kir4.1. Findings suggest that the therapeutic effect of YGMMD in DME is probably due to the deregulation of AQP4/Kir4.1 expression through the ERK1/2-PI3K-AKT pathway. Conclusion: This study shows that YGMMD inhibits the activation of p-ERK1/2 while concurrently enhancing the expression of p-AKT, leading to a decrease in AQP4 levels and the upregulation of Kir4.1 expression. As a result, the balance in the retinal fluid clearance system is restored, effectively alleviating DME.

Keywords: Diabetic retinopathy, molecular docking, experimental verification, water balance

Introduction

The retina is a crucial sensory tissue in the human body that requires precise fluid balance to maintain cellular homeostasis and normal tissue function. High-throughput water transport through aquaporin (AQP) proteins on the cell membrane is an important molecular process that positively regulates glandular tissue fluid secretion. This process promotes fluid exchange of nutrients and metabolic products between the intracellular and extracellular environments and regulates cell volume by maintaining water balance [1, 2]. The formation of diabetic macular edema (DME) is closely related to the balance of fluid in the macular region. An imbalance between the volume of fluid in and out and the water permeability of the retina leads to fluid accumulation in the retina, causing retinal edema, which ultimately affects the central fovea of the macula and severely affects the patient's visual function [3].

Müller cells, which account for 95-97% of the entire retinal structure, are glial cells responsible for the rapid transport of fluid in the retina and the timely removal of excess fluid [4]. Their primary function is to accelerate aqueous fluid transport in the retina, promoting the flow of fluid towards the vitreous body or blood vessels, thereby maintaining aqueous fluid homeostasis in the retina and ensuring the relative dehydration of retinal tissues. The normal func-

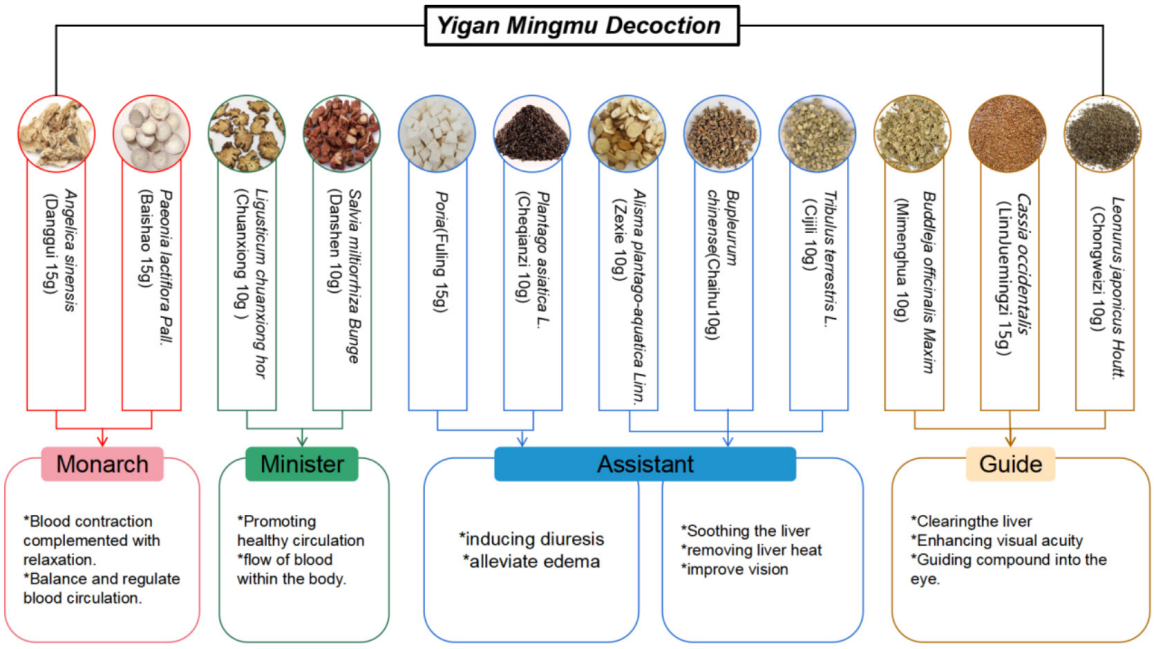

Figure 1. The compositions of Yigan Mingmu Decoction and their efficacy.

tion depends on the expression and distribution of pathway-related proteins aquaporin 4 (AQP4) and inwardly-rectifying potassium channel subtype (Kir) 4.1 (Kir4.1) on the Müller cell membrane [5-7].

AQP4 is highly expressed on Müller cell membranes. The transport of water molecules through AQP4 is driven by transmembrane osmotic pressure or static water pressure, particularly by the ion concentration gradient caused by the uneven distribution of potassium ions [8]. Kir4.1 is the main channel protein for the inward transport of potassium ions that specific to Müller cells [9, 10]. Both AQP4 and Kir4.1 are components of the Müller cell volume regulation network [11]. The dystrophin (DP)71 protein complex anchors Kir4.1/AQP4 to the foot processes of Müller cells in the retina, and they exhibit a coupled relationship in terms of structure and function [12]. Diabetes - induces DR, which exacerbates retinal ischemia and hypoxia and results in abnormalities in the expression and function of AQP4 and Kir4.1 [13], eventually leading to retinal edema.

Our research team has formulated Yigan Mingmu Decoction (YGMMD) as a therapeutic modality for addressing diabetic macular edema (**Figure 1**). Cystoid macular edema is believed to be caused by the swelling and death of Müller cells [6]. In our clinical practice, it was evident that YGMMD treatment results in a notable amelioration of cystoid macular edema (**Figure 2**).

In our previous study, we found that YGMMD could target and protect Müller cells under high-glucose conditions [14-16]. Clinical randomized controlled trials have demonstrated that YGMMD can alleviate DME [14]. Research has confirmed that YGMMD can reduce blood glucose levels in DME model rats and alleviate retinal edema. It was found that YGMMD can reduce recombinant thioredoxin-interacting protein (TXNIP) expression in Müller cells, thereby preventing cell apoptosis [15]. It was also found that YGMMD can down-regulate the protein expression of NOD-like receptor thermal protein domain associated protein 3 (NLRP3), Apoptosis-associated speck-like protein containing a CARD (ASC), and Cysteinyl aspartate specific proteinase-1 (Caspase-1), and inhibits the release of the inflammatory factors interleukin-1 (IL-1) and interleukin-18 (IL-18), thereby preventing cell pyroptosis, improving the inflammatory state of retinal tissue, alleviating retinal pathologic damage, and delaying the progression of DME [16].

Although clinical and experimental studies have highlighted the potential of YGMMD in the

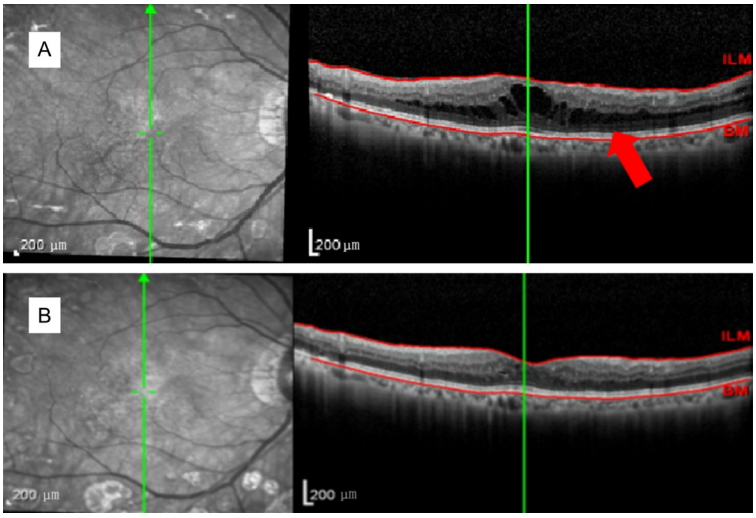

Figure 2. (A) Swelling in Müller cells in diabetic macular edema patient before (A) and after the treatment (B). The arrows on the image indicate swelling within Müller cells.

treatment of DME, additional evidence from animal studies is essential to gain a deeper understanding of the mechanisms underlying the effect of YGMMD on progression.

In this study, we used network pharmacology to identify the active ingredients and gene targets associated with YGMMD. Our findings suggest that YGMMD may modulate the expression of AQP4 through the phosphorylase extracellular regulated protein kinase (p-ERK1/2)-Phosphatidylinositol 3 kinase (PI3K)-protein kinase B (AKT) signaling pathway.

Materials and methods

Network pharmacological analysis

Prediction of drug and disease-related targets: To identify the compounds in YGMMD, we searched the Traditional YGMMD Systems Pharmacology Database and Analysis Platform (TCMSP, V2.3) [17]. We used oral bioavailability and drug similarity indices to search for active ingredients in the TCMSP database. We then used the TCMSP database to search for the relevant targets of YGMMD, and standardized the targets using the UniProt database [18], obtained their official names (official symbols) and established a dataset. Next, we identified the relevant targets of DME from GeneCards [19] and OMIM databases [20] to obtain disease-related targets.

Screening of common targets of diseases and drugs and construction of protein-protein interaction (PPI) network: The biologically active ingredients of YGMMD and disease targets of DME were imported into an online drawing website [21] to obtain intersection genes for visualization. This intersection indicates possible targets of YGMMD for treating DME. We then analyzed the biologically active ingredients and targets of YGMMD using the Cytoscape 3.7.2 software [22], drew a network of active ingredient targets and identified the factors that may play a crucial role in YGMMD treating DME.

To further investigate the PPI in the treatment of DME with YGMMD, the obtained drug-disease intersection genes were imported into the online STRING 11.5 database [23]. The network parameters were output in "tsv" format and imported into Cytoscape 3.7.2 for network analysis. The PPI network diagram of core targets was obtained, and the CytoHubba plugin was used to calculate the topological parameters of each target in the PPI network. The top 10 targets were selected, and the shared targets were the key targets for YGMMD treatment of DME.

Gene Ontology (GO) and Kyoto Encyclopedia of Genes and Genomes (KEGG) enrichment analysis: We imported the co-targeted genes that intersected by drugs and diseases into Metascape [24] at a significance level of $P < 0.05$. We conducted PPI, GO, and KEGG enrichment analyses to demonstrate molecular mechanisms and key GO and KEGG pathways. Bubble charts were generated for each analysis. Pathview, an R package for visualizing KEGG pathways, was used to visualize gene enrichment.

Molecular docking: Molecular docking was performed using crystal structures obtained from the PDB database [25]. The 3D structures of small molecules were obtained from the PubChem database, and energy minimization studies were carried out using the MMFF94

force field. In this study, molecular docking analysis was performed using AutoDock Vina 1.1.2 software [23] and all receptor proteins were processed using PyMol 2.5 [26], before submitting them for docking.

Experimentation on animals

Animals: A total of 48 healthy male, Sprague-Dawley (SD) rats aged 2 months and weighing (200±10) g were used. The rats had no ocular diseases and were raised in a specific pathogen-free (SPF) animal center (43072720110-103196) provided by Hunan SLC Jingda Experimental Animal Co., Ltd. Our experimental plan involving animal care was approved by the Experimental Animal Care and Use Committee of Hunan University of Traditional YGMMD (Approval No.2020-0060) and followed the guidelines for the care and use of laboratory animals of the National Institutes of Health (NIH).

Model establishment: Following two weeks of adaptive feeding, the model group received an intraperitoneal injection of a freshly prepared blend of citric acid buffer (pH=4.2-4.5) and STZ to create a 1% Streptozocin (STZ) solution (40 mg/kg) (Sigma, Beijing, lot: 08E221108) [27]. After 72 hours, the random blood glucose levels of the model group were measured. Rats with random blood glucose levels ≥ 16.8 mol/L were considered to have successfully modeled diabetes. All model groups were fed a high-sugar, high-fat diet. In the 8th week following modeling, the success of the model was verified.

Drug treatment: After building the diabetic retinopathy (DR) model, the rats (n=30) were randomly assigned to five groups: model (i.e., deionized water), YGMMD-H (12.2 g/kg), YGMMD-M (5.6/kg), YGMMD-L (2.8 g/kg) (Chenguang Jiuhui, Hunan), and Andomine (0.09 mg/kg) (Tianan, Guizhou, log: 1420-1658642). All groups underwent a four-week intervention. Gavage was used to provide an identical volume of physiologic saline to that of the control group.

General morphology, blood glucose, and body weight examination: To evaluate the biological differences between the control and model groups, findings such as fur, physique, reactions, eating and drinking habits, and excretion were measured. In addition, the degree of lens opacity was assessed to determine whether metabolic cataracts occur as the disease progresses. Blood glucose and body weight were measured randomly before and after modeling, during the first, second, fourth, and eighth weeks of diabetes, and before and after gavage for the first, second, third, and fourth weeks.

Optical coherence tomography (OCT) measures retinal thickness: Before and at the 4th and 8th week after drug intervention, OCT was performed to measure and compare the retinal thickness of the rats at a distance of 2DD from the optic disc, which was manually measured using the system's measurement software.

Fluorescence fundus angiography (FFA) fundus fluoroscopy: After the 4th and 8th week post-molding, an FFA examination was performed. For the examination, a 20% quality fraction of fluorescein sodium (0.012 mL/g) was injected into the rat's abdominal cavity, and the rat's retinal blood vessels were continuously photographed to observe the filling status of the blood vessels. Vascular density analysis was conducted using AngioTool software [28].

Assessment of hematoxylin and eosin (H&E) staining and Müller cell edema: After successful anesthesia, the optic nerve was dissected, and the rat's eyeball was removed and fixed in an eyeball fixation solution. Samples were embedded in paraffin, stained with hematoxylin, and rinsed with Phosphate Buffer Saline (PBS). Subsequently, the samples were stained with eosin then dehydrated using a gradient of alcohol (95-100%). They were then fixed twice in xylene and sealed with a neutral resin after mounting on a slide. The evaluation of intracellular edema in the Müller cells of the retina was performed according to previously published methods, and the swollen morphology of the Müller cells was examined under an optical microscope.

Double-label immunofluorescence: Retinal samples were stained with primary antibodies against AQP4 (Santa Cruz, USA, catalog number: Sc-32739) and Kir4.1 (Proteintech, USA, catalog number: 12503-1-AP). Incubation overnight at 4°C was followed by the application of a secondary antibody. Following this, phenylindole (DAPI) staining was performed. After storage in the dark, tissue images were acquired using a fluorescence microscope.

Immunohistochemical analyses: Retinal samples were subjected to immunostaining using a primary antibody against p-ERK1/2 (catalog number: ab214362; Abcam, UK), followed by the application of a secondary antibody and incubation overnight at 4°C. Subsequently, Diaminbiphenyl (DAB) staining was performed. Finally, tissue images were acquired using a fluorescence microscope.

Western blot: The protein concentration was determined using the Bicinchoninic Acid (BCA) method. A total of 80 μL of protein supernatant was transferred to a membrane and blocked with 5% skim milk at room temperature for 1.5 hours. Primary antibodies against AQP4 (1:100), Kir4.1 (1:500), p-ERK1/2 (1:100), protein kinase B (AKT) (1:1000), p-AKT (1:5000), and phosphatidylinositol 3 kinase (PI3K) (1:5000) were used. The cells were incubated overnight at 4°C. The samples were washed three times with PBST for 10 min each. Horseradish Peroxidase (HRP) goat anti-mouse IgG (1:5000) and HRP goat anti-rabbit IgG (1:6000) were used as secondary antibodies. The cells were incubated at room temperature for 1.5 hours, washed three times with PBS+ Tween-20 (PBST) for 10 min each, and visualized with enhanced chemiluminescence (ECL). Image J software was used to perform grayscale analysis of protein bands and express the relative protein expression level as the ratio of the grayscale value of the target protein to that of β-actin.

Statistical method

Experimental data were analyzed using SPSS software (version 26.0). The quantitative variables were expressed as the mean ± standard deviation. Prior to conducting multiple comparisons using analysis of variance (LSD) and Dunnett's methods, the normality and homogeneity of variance were assessed. If normality and homogeneity of variance assumptions were met, variance analysis was performed; otherwise, non-parametric multiple comparisons were performed. Counted data were analyzed using the χ^2 test, and data with heterogeneous variances were analyzed using the rank-sum test. Statistical significance was set at $P < 0.05$, with a threshold of $P < 0.01$ for highly significant differences.

Results

Network pharmacology

Prediction of drug and disease-related targets: We screened active compounds in TCMSP. Using the results from the database, we identified 175 active compounds in YGMMD. We then extracted the targets of these active compounds from the TCMSP database and merged them to exclude duplicates, resulting in a total of 289 targets.

The network diagram for the "Drug Target" was generated using Cytoscape 3.7.2 software, and the primary active ingredients of YGMMD were analyzed using the network analyzer function. Quercetin, apigenin, and kaempferol exhibited the highest values (**Figure 3**).

Screening of common targets of diseases and drugs and construction of PPI network: A search of the GENECARD and OMIM databases identified 830 targets associated with DME. After combining the data from both databases and eliminating duplicates, 89 overlapping targets were identified by comparison with YGMMD targets. The resultant protein-protein interaction (PPI) network was derived from the shared targets of YGMMD and DME.

We analyzed the degree, betweenness, and closeness of topologic values for the PPI network targets using the CytoHubba plugin in Cytoscape 3.7.2, which presented the information and interactions of the top ten targets across the three parameters, including tumor protein p53 (TP53), AKT1, tumor necrosis factor (TNF), Caspase-3 (CASP3), vascular endothelial growth factor (VEGFA), and interleukin 6 (IL6). Notably, these five targets were highly ranked in all three parameters, indicating that they may be crucial targets for YGMMD treatment of DME (**Figure 4**).

GO and KEGG enrichment analysis: GO functional enrichment analysis was conducted to identify biological processes (BP), cellular components (CC), and molecular functions (MF), and KEGG pathway enrichment analysis of the co-targets was performed using R software (**Figure 5**).

Molecular docking: The results of molecular docking revealed the degree of binding activity between the key components and targets, and

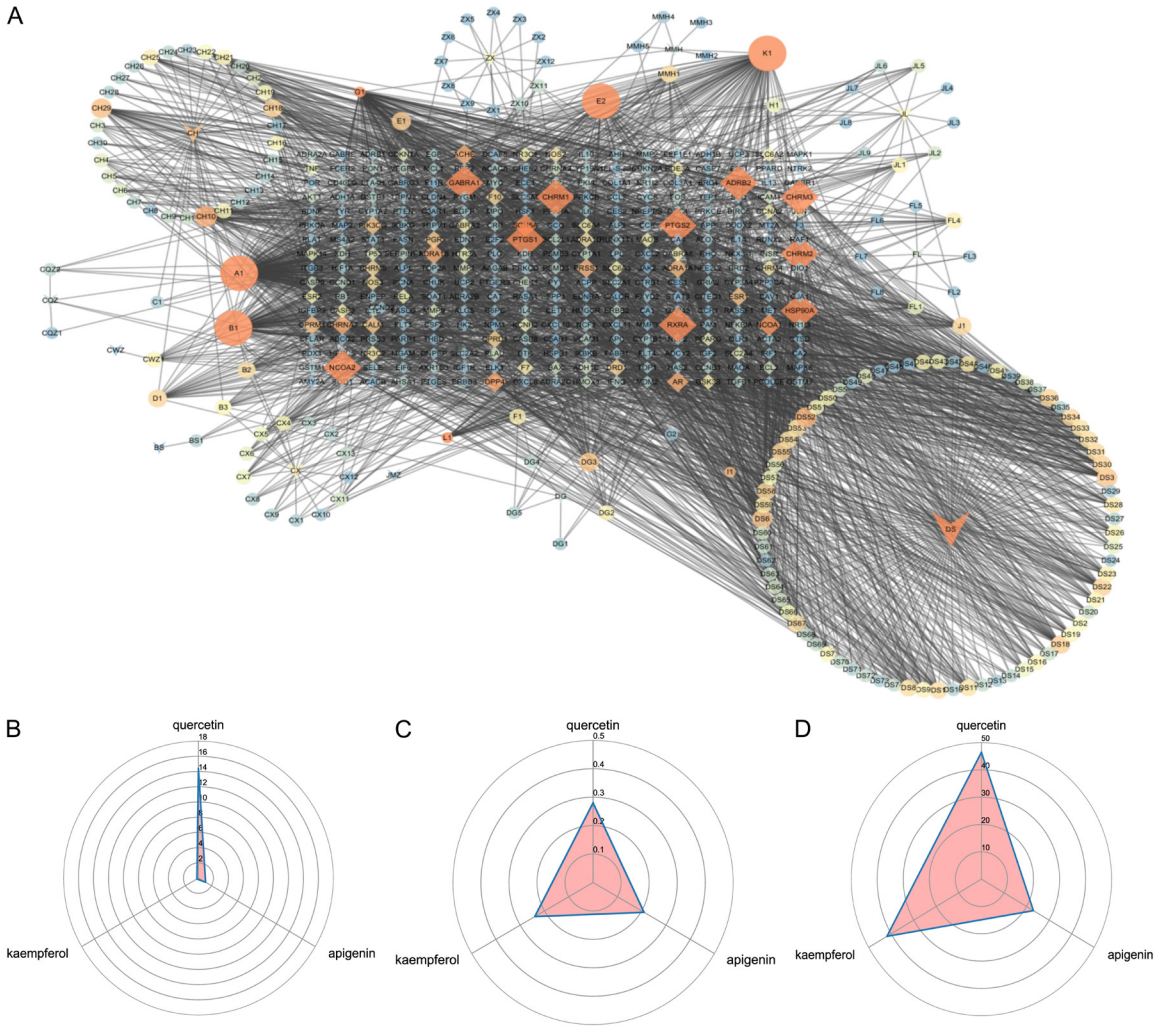

Figure 3. Prediction of drug and disease-related targets. A: Target map of effective active components of Yigan Mingmu Decoction (YGMMD). B: Drug half-life. C: Drug-likeness. D: Oral-bioavailability.

the docking results depicted the interaction between the components exhibiting favorable binding activity and their respective targets (**Figure 6**).

Experimentation on animals

Model validation: After the successful modeling through STZ injection, the rats gradually began exhibiting symptoms such as slow body weight gain, hair loss, and the lenses of rats in the model group became progressively cloudy (**Figure 7**).

Compared to the control group, blood glucose levels in the model group increased and stabilized within three days, remaining consistently elevated during the weeks following post-modeling ($P < 0.01$). Their weights were lower than those of the control group after post-modeling ($P < 0.01$) (**Figure 8**). The retinal thickness in both eyes of the model group was significantly increased after modeling ($P < 0.05$) (**Figure 9**).

After eight weeks of modeling, some capillaries in the modeling group appeared disordered and occluded, and microvascular tumors were found, accompanied by obscured fluorescence (**Figure 10**). The retinal vascular density was analyzed using Angiotool 64.0, which revealed that the vascular density in the model group was significantly higher than that in the control group ($P < 0.01$) (**Figure 11**).

In the model group, after 4 weeks of modeling, the retinal structure was relatively disordered,

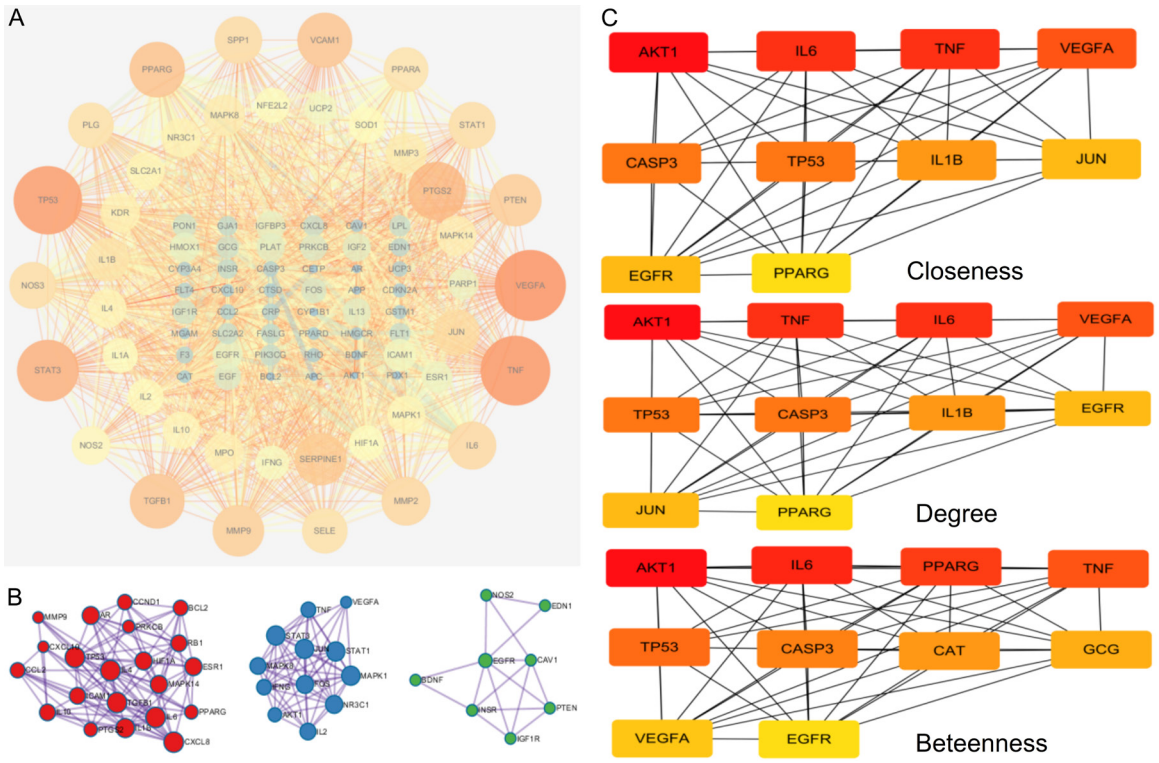

Figure 4. Screening of common targets of diseases and drugs and construction of Protein-protein interaction (PPI) network. A: PPI network diagram; B: Gene cluster analysis and core target screening; C: The top 10 targets ranked by degree, betweenness, closeness, and their interaction information.

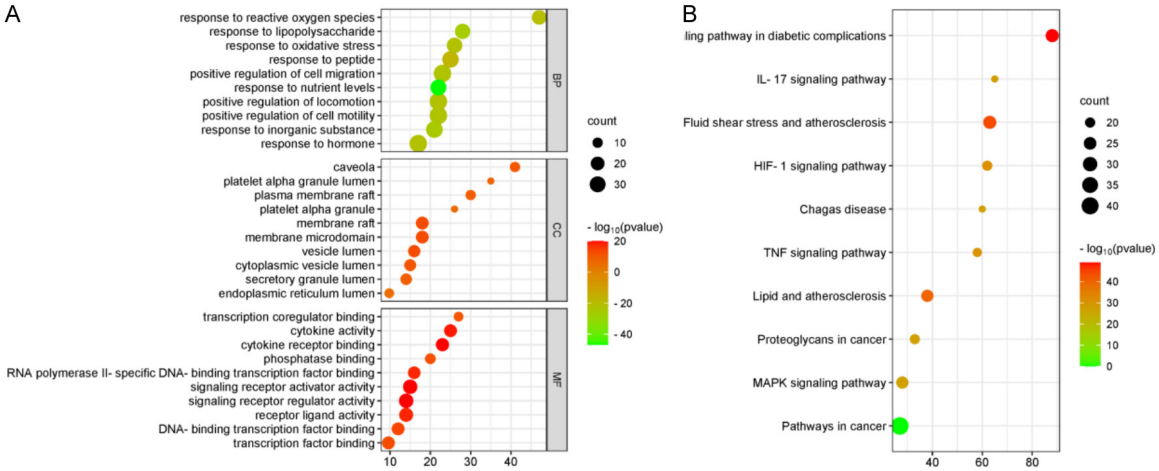

Figure 5. Gene Ontology (GO) annotation (A) and Kyoto Encyclopedia of Genes and Genomes (KEGG) pathway (B) analyses.

with some cells showing vacuolar changes, whereas after 8 weeks of modeling, the nerve fiber layer was swollen and arranged disorderly (**Figure 12**).

YGMMD reduced blood sugar and promoted body weight gain in rats: The other four groups that received drug treatment had lower blood glucose levels than the model group (all $P <$

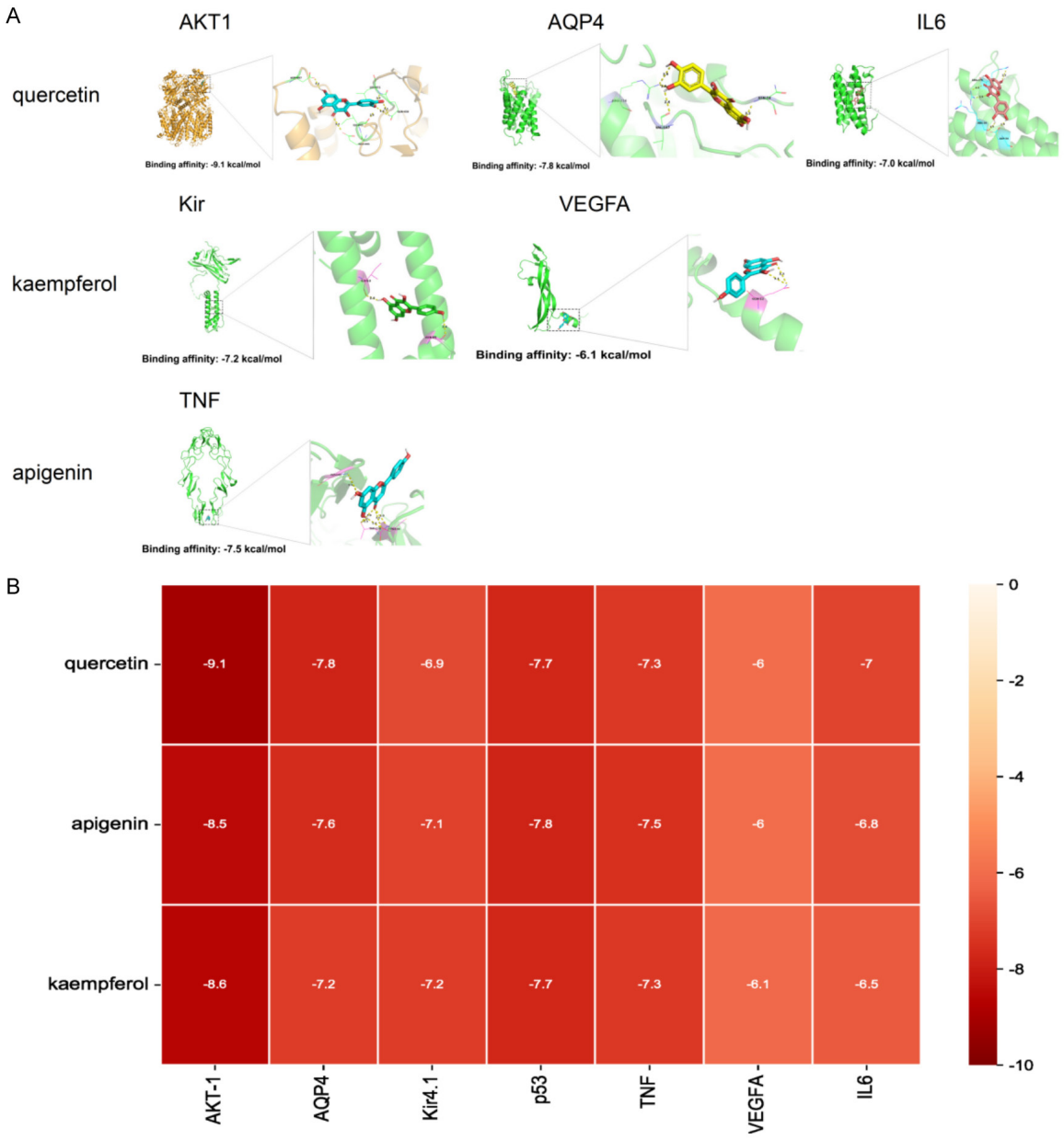

Figure 6. Certain binding activity between the key components and targets. A: High-affinity target molecule docking; B: Molecular docking and binding energy.

0.05). The drug treatment groups showed higher weights than the model group, displaying a gradual upward trend (**Figure 13**).

YGMMD reduced retinal thickness and Muller intracellular edema in rats: Compared to the model group, the intracellular edema of Müller cells was alleviated after treatment with YGMMD in all groups. Among the four drug-intervention groups, retinal thickness in the medium-dose YGMMD group decreased the most significantly ($P < 0.05$) (**Figure 14**).

YGMMD down-regulated AQP4 and up-regulated Kir4.1 expression: Protein expression of retinal AQP4 and Kir4.1 of rats was tested using western blot and immunofluorescence double-labeling.

In the model group, AQP4 expression was significantly higher compared to the control group ($P < 0.05$) and lower compared to the andomine group ($P < 0.01$).

Among the four drug-intervention groups, the AQP4 protein levels decreased significantly.

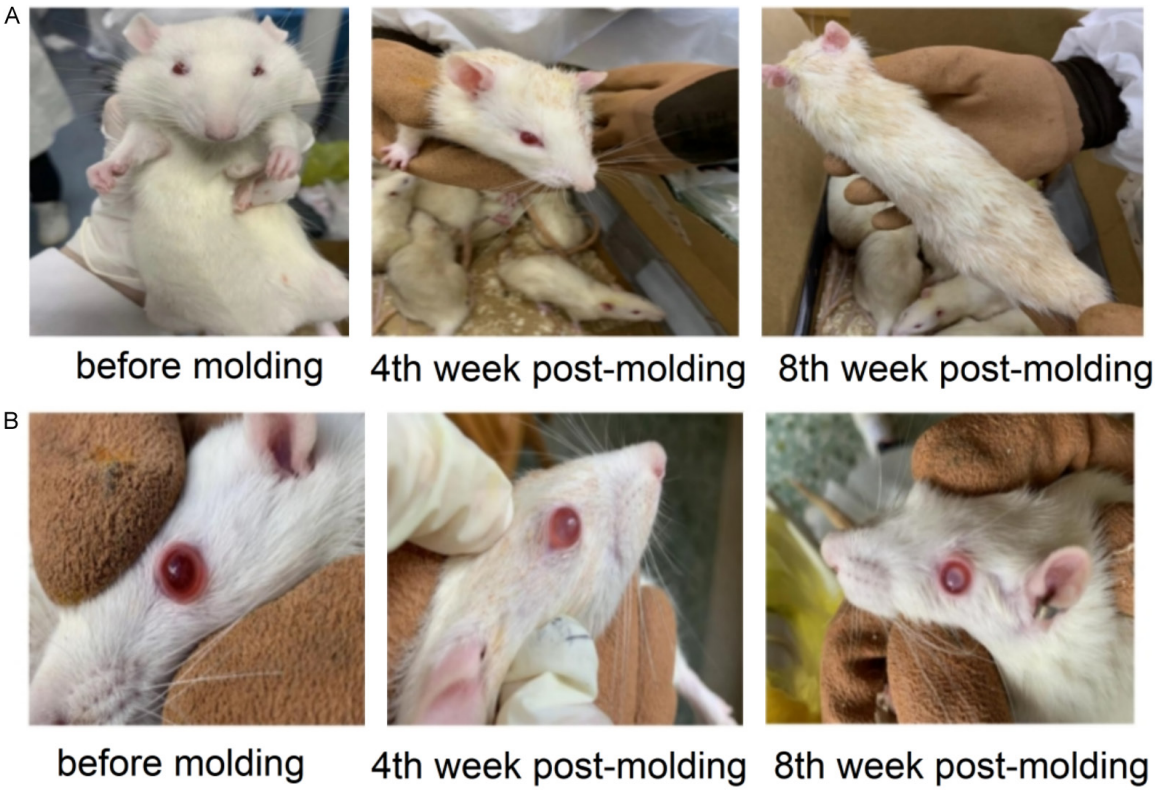

Figure 7. Slow weight gain, hair loss and wilting, and cloudy lenses were observed in the rats of model group. A: Changes in hair and weight in the rats of model group; B: The changes in lenses in the rats of model group.

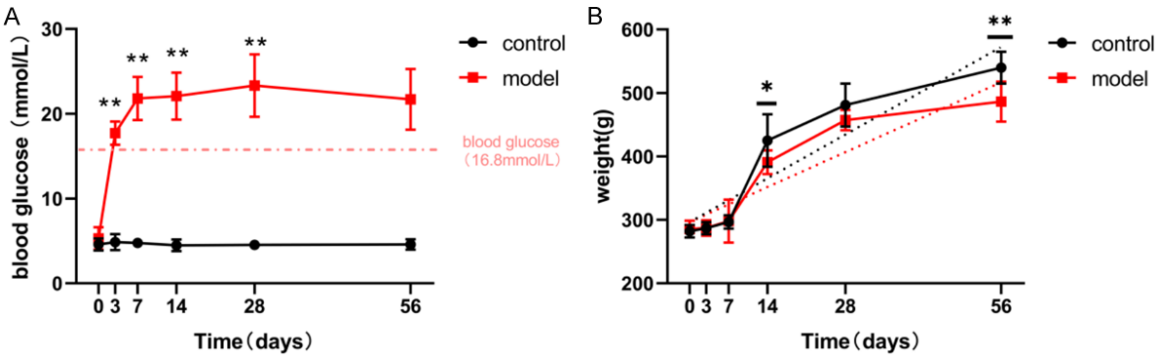

Figure 8. Changes in blood glucose levels (A) and body weight (B) at different time points during the modeling stage. *P < 0.05 vs. control; **P < 0.01 vs. control.

Notably, the YGMMD-M group demonstrated the lowest AQP4 expression in rat retinas, surpassing that of the positive control groups (P < 0.05).

Conversely, the model group displayed lower Kir4.1 expression compared to the control group (P < 0.05). The model group displayed a higher Kir4.1 expression compared to the andomin group (P < 0.01). Among the four drug-intervention groups, the YGMMD-M group exhibited a higher Kir4.1 expression than the positive drug group (P < 0.05) (**Figures 15**, **16**).

YGMMD regulates the ERK1/2-PI3K-AKT signaling pathway: Compared to the control group, the model group exhibited higher p-ERK1/2 expression (P < 0.05). Compared to the model group, the andomine group exhibited lower p-ERK1/2 expression (P < 0.01). Among the

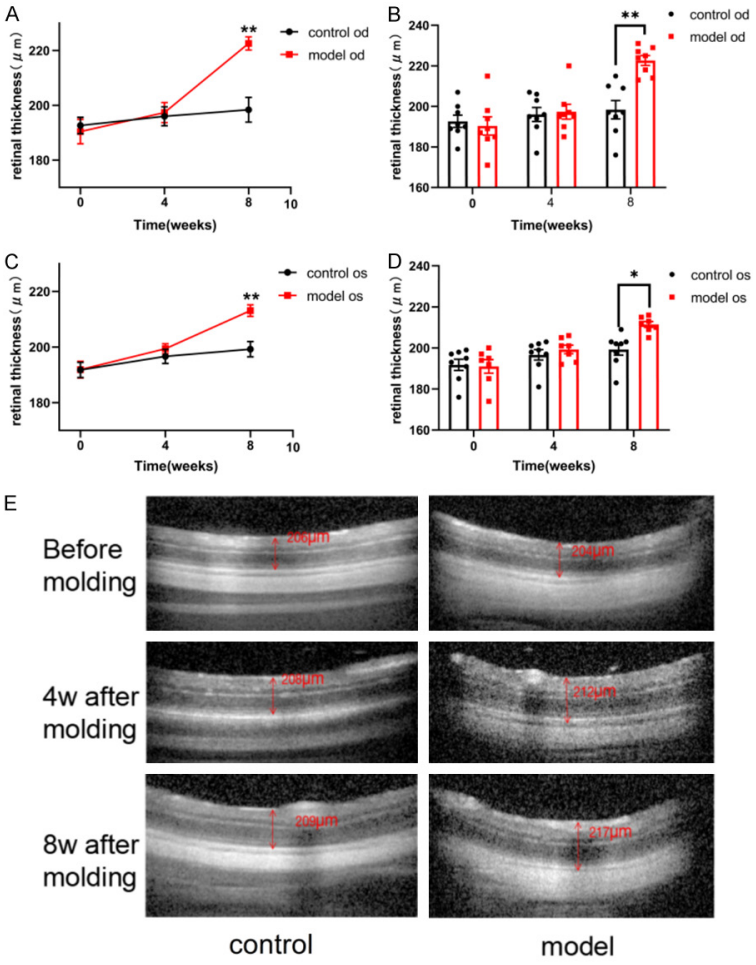

Figure 9. The retinal thickness of the model group was increased after modeling. A and B: Retinal thickness of the oculus dexter at different time points during the modeling stage; C and D: Retinal thickness of the oculus sinister at different time points during the modeling stage; E: Retinal thickness measured by Optical coherence tomography (OCT). *P < 0.05, vs. control; **P < 0.01, vs. control.

four drug-intervention groups, the protein expression of p-ERK1/2 was the lowest in the YGMMD-M group (P < 0.05).

To verify the accuracy of the western blot results, we used immunohistochemistry to detect the expression levels of p-ERK1/2 in the rats' retinas. Compared to the other five groups, the expression of p-ERK1/2 in the model group was the highest (P < 0.05). Among the four drug intervention groups, the expression of p-ERK1/2 in the YGMMD-H group was lower than that of all other groups (P < 0.05) (**Figures 17**, **18**).

Combining the experimental results, the medium dose of the YGMMD was optimal for therapeutic use. AKT, p-AKT, and PI3K levels in the control group were significantly higher than those in the model group (P < 0.01). The expression levels of p-AKT, AKT, and PI3K in the model group were lower than those in the YGMMD-M group (P < 0.05; P < 0.01, respectively) (**Figure 19**).

Discussion

Diabetic macular edema (DME) is a prevalent and chronic microvascular complication stemming from diabetes mellitus (DM), and may cause irreversible vision impairment. The decrease in the retinal fluid clearance rate is considered the underlying cause of macular edema [3]. AQP4 and Kir4.1, which co-localize within the foot processes of Müller cells proximate to the retinal vasculature, substantially influence the maintenance of retinal fluid homeostasis and preservation of retinal tissue in a relatively desiccated state [1, 2]. Our experimental results showed that YGMMD can downregulate the expression of AQP4 while upregulating Kir4.1 expression. Therefore, YGMMD may alleviate diabetic macular edema by modulating the retinal fluid clearance rate (**Figure 20**).

In clinical practice, YGMMD has demonstrated significant advantages in stabilizing the condition of patients with DME [14]. However, its multi-target, multi-component, and multi-pathway nature makes it challenging to determine which components play a primary role in treating the disease. Leveraging current biology techniques and research findings can be used to integrate network pharmacology and study the specific mechanisms and compatibility patterns of traditional Chinese medicine formulations. Our previous studies have confirmed the safety and effectiveness of YGMMD for the treatment of DME [15, 16].

AQP4 is an integral member of the aquaporin protein family responsible for water channel activity. Bordoni found that loss of AQP4

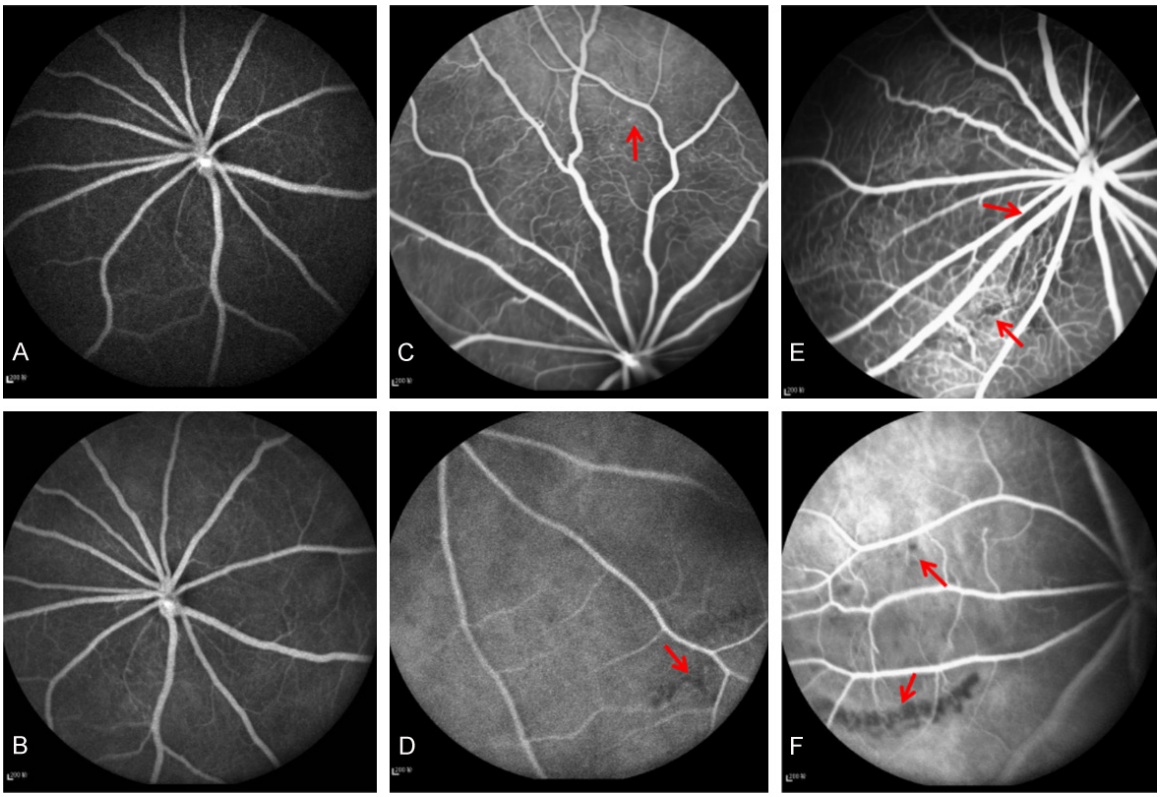

Figure 10. The observation of capillaries in control group and model groups. A and B: Control group at 8th week after modeling; C and D: Model group at 4th week after modeling; E and F: Model group at 8th week after modeling.

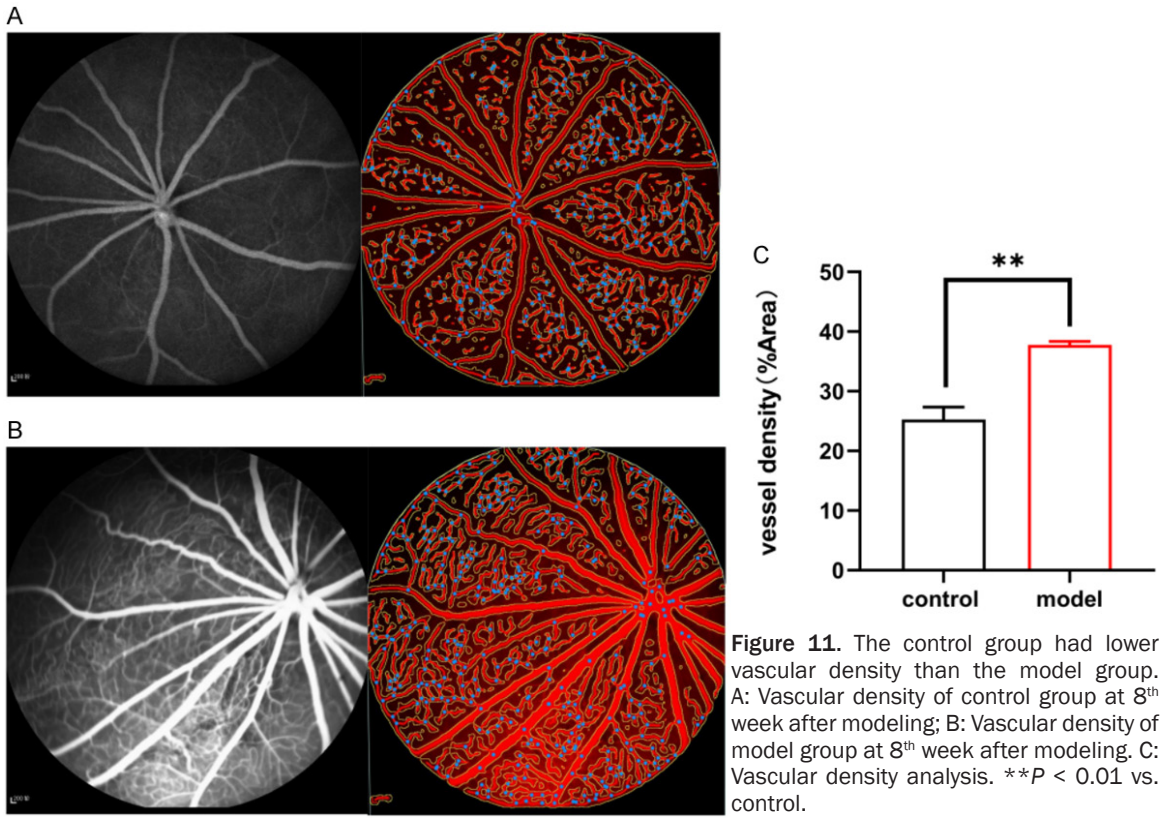

Figure 11. The control group had lower vascular density than the model group. A: Vascular density of control group at 8th week after modeling; B: Vascular density of model group at 8th week after modeling. C: Vascular density analysis. $^{**}P < 0.01$ vs. control.

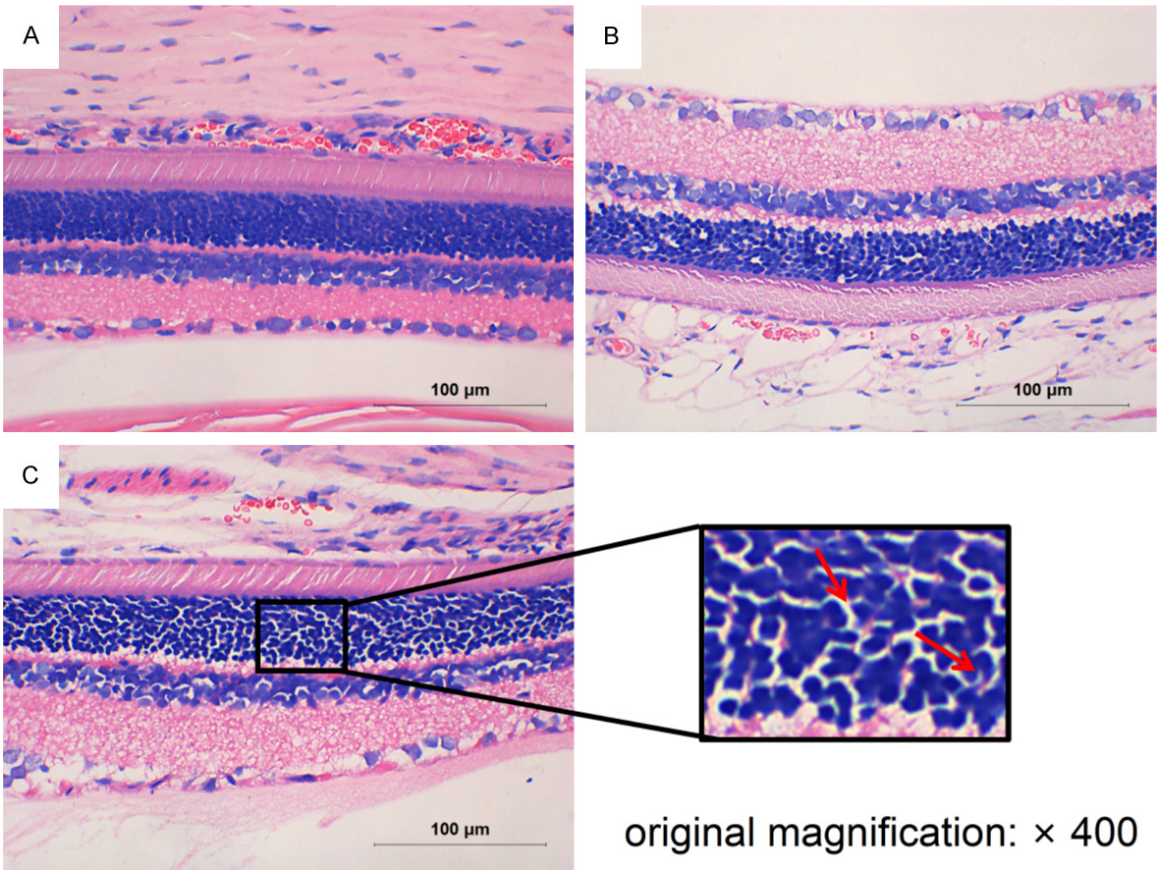

Figure 12. Histopathologic observation of the retina of rats (H&E staining, ×400). A: Before modeling; B: 4 weeks after modeling; C: 8 weeks after modeling.

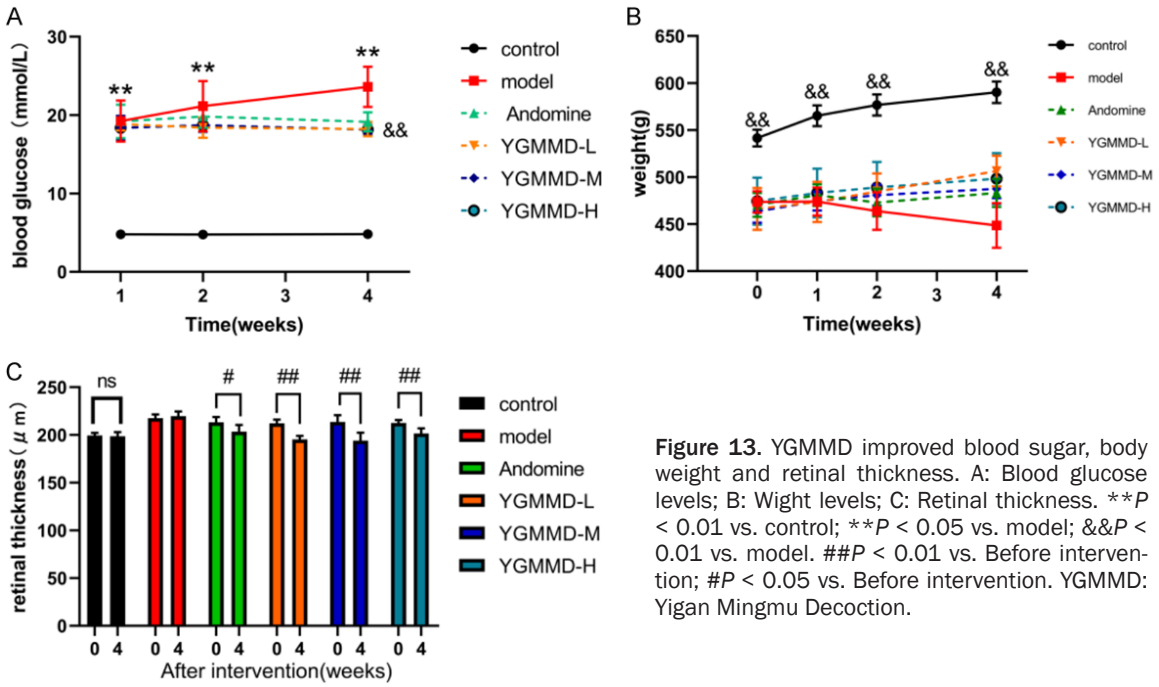

Figure 13. YGMMD improved blood sugar, body weight and retinal thickness. A: Blood glucose levels; B: Wight levels; C: Retinal thickness. $^{**}P < 0.01$ vs. control; $^{**}P < 0.05$ vs. model; &&$P < 0.01$ vs. model. ##$P < 0.01$ vs. Before intervention; #$P < 0.05$ vs. Before intervention. YGMMD: Yigan Mingmu Decoction.

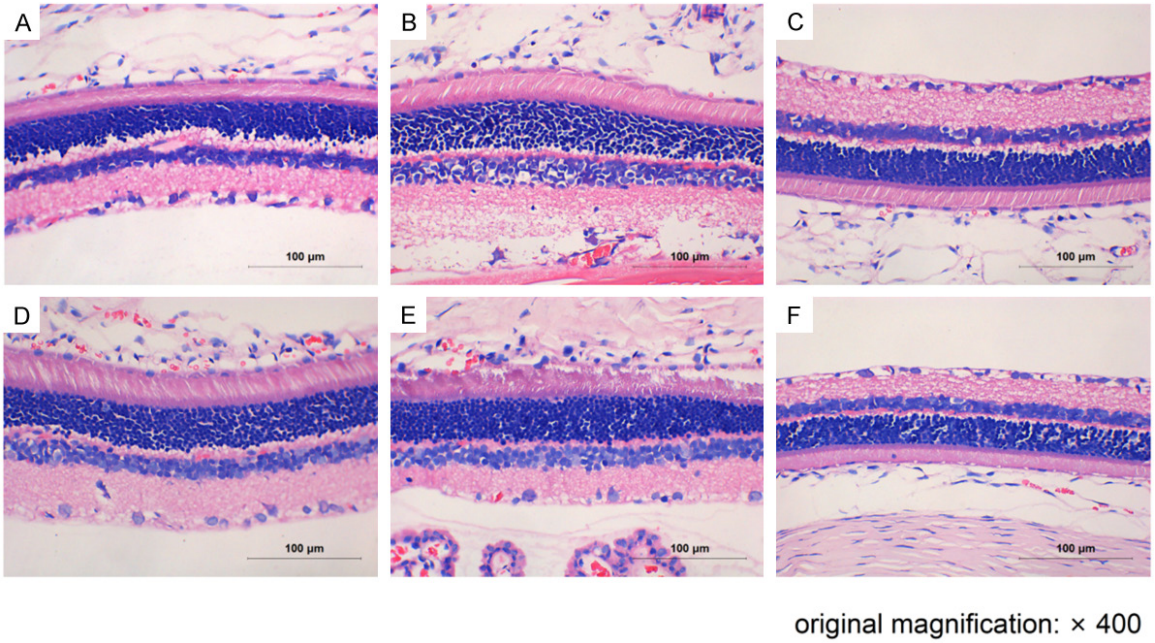

Figure 14. YGMMD and Adomine effectively alleviated retinal edema as observed by H&E staining (×400). A: Control group; B: Mode group; C: Adomine group; D: YGMMD-L; E: YGMMD-M; F: YGMMD-H. YGMMD: Yigan Mingmu Decoction.

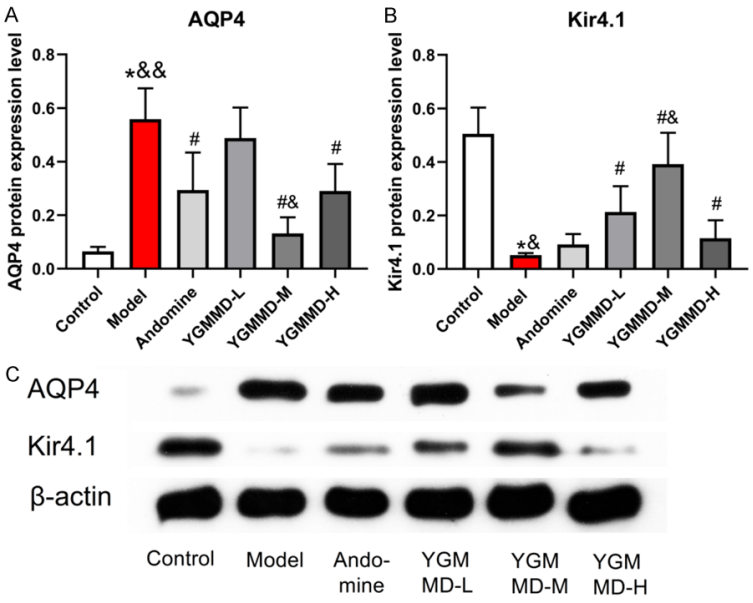

Figure 15. Expression of AQP4 and Kir4.1 proteins in the retinal tissues of the rats in different groups. A: Quantitative analysis of expression levels of AQP4; B: Quantitative analysis of expression levels of Kir4.1; C: Western blots for AQP4 and Kir4.1. *P < 0.05, vs. Control; #P < 0.05, vs. Model; &P < 0.05, vs. Andomine; &&P < 0.01, vs. Andomine.

improves cell edema [29]. Kir4.1, a principal channel protein, serves as a specific inward transporter of potassium ions (K^+) within Müller cells [7]. Djukic and Netti found that when exposed to a high-glucose environment, Kir4.1 expression decreased, leading to an increase in the extracellular concentration of K^+ ions. This, in turn, causes the depolarization of Müller cells [30, 31]. Consequently, water molecules enter Müller cells in large quantities through AQP4 channels, causing cellular swelling. Fang found that a high-glucose environment can lead to up-regulation of AQP4 expression and down-regulation of Kir4.1 expression, which is consistent with the results of this experiment [32]. Interestingly, our results suggest that the up-regulated level of AQP4 and the down-regulated level of Kir4.1 basically converge, and suggest that AQP4 and Kir4.1 may regulate the balance of retinal water metabolism through a synergistic effect. Previous studies have also shown that the expression of Kir4.1 may be negatively correlated with the expression of

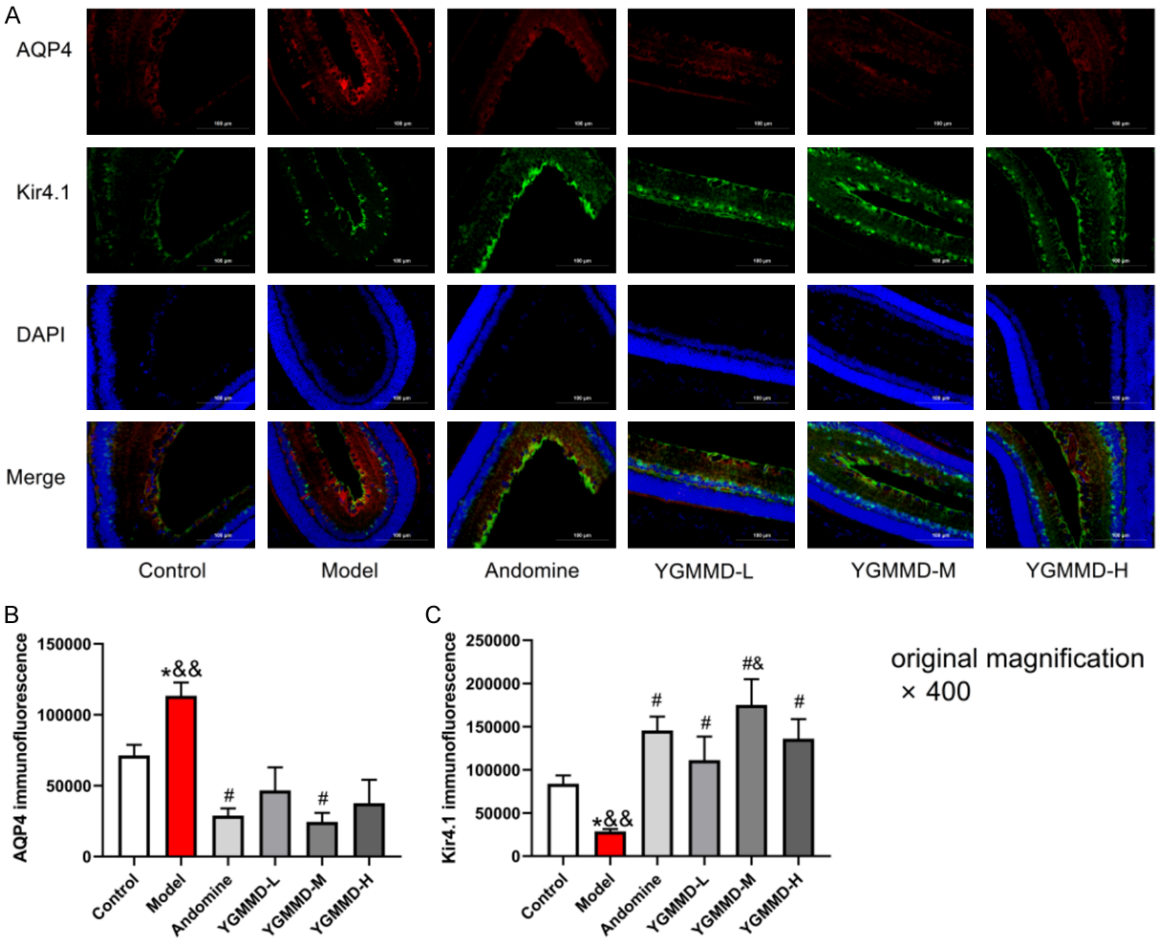

Figure 16. YGMMD reduced the deposition of AQP4 in retinal tissue of rats but increased the deposition of Kir4.1 as observed under immunofluorescence microscopy (400×). A: Immunofluorescence for AQP4 and Kir4.1; B: The fluorescence intensity of AQP4 was quantified; C: The fluorescence intensity of Kir4.1 was quantified. *$P < 0.05$, vs. control; #$P < 0.05$, vs. Model; &$P < 0.05$, vs. Andomine; &&P < 0.01, vs. Andomine. YGMMD: Yigan Mingmu Decoction; AQP4: aquaporin 4; Kir4.1: inwardly rectifying potassium channel subtype 4.1; DAPI: phenylindole.

AQP4 [5, 31], and Jiang found that KIR4.1-mediated cell retraction is related to AQP4 activity [33]. Elsherbini found that the expression of AQP4 was positively correlated with water content, and the expression of Kir4.1 was negatively correlated with water content [34].

Kim found that the ERK1/2-PI3K-AKT signaling pathway in Müller cells can regulate AQP4/KIR4.1 [35]. Prolonged exposure to hyperglycemic conditions can impede the function of Kir4.1 channels while simultaneously activating the P-ERK1/2 signaling pathway [36]. This molecular cascade leads to the upregulation of AQP4 expression [37]. Inhibiting the activation of ERK1/2 can activate the phosphorylation of AKT in the cell [38], thus down-regulating the expression of AQP4 and activating Kir4.1 expression [39, 40]. Interestingly, the ERK1/2 and PI3K/AKT pathways show mutual regulation, including cross-inhibition and cross-activation [41-43].

Based on network pharmacology results and molecular docking predictions, the main active components of YGMMD (quercetin, apigenin, and kaempferol) may act on AKT1, AQP4, and Kir4.1 for the treatment of DME. KEGG analysis suggested that YGMMD regulates the progression of DM and insulin levels through various signaling pathways, including the AGE-RAGE signaling pathway and insulin resistance. The latest research supports our hypothesis, showing that the main active components of YGMMD (quercetin, apigenin, and kaempferol)

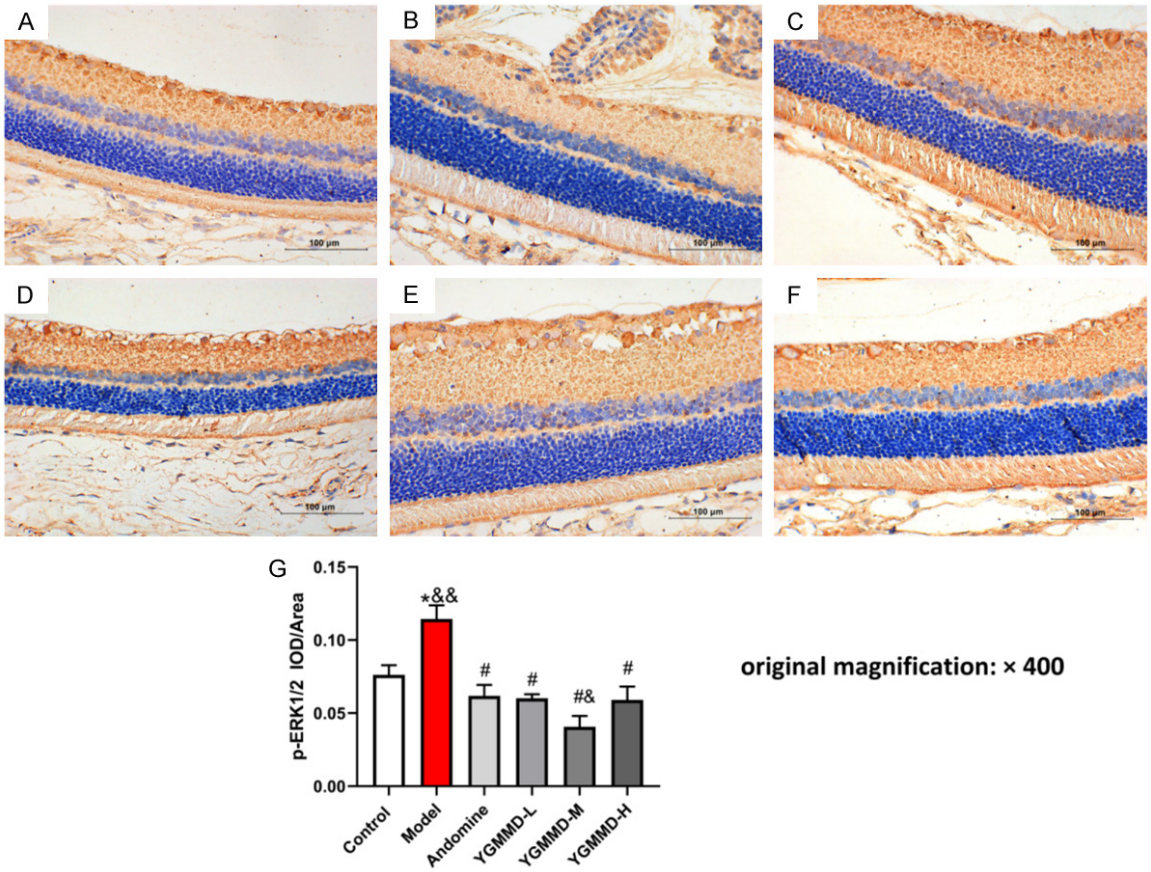

Figure 17. Immunohistochemistry (×400) revealed that the deposition of p-ERK in retinal tissue of rats treated with YGMMD was reduced. A-F: Retinas of rats in the blank group, model group, Andomine group, YGMMD-L group, YGMMD-M group, and YGMMD-H group at 8th week after modeling, respectively. G: Quantification of p-ERK IOD/Area. *P < 0.05, vs. Control; #P < 0.05, vs. Model; &P < 0.05, vs. YGMMD-H; &&P < 0.01, vs. Andomine. YGMMD: Yigan Mingmu Decoction.

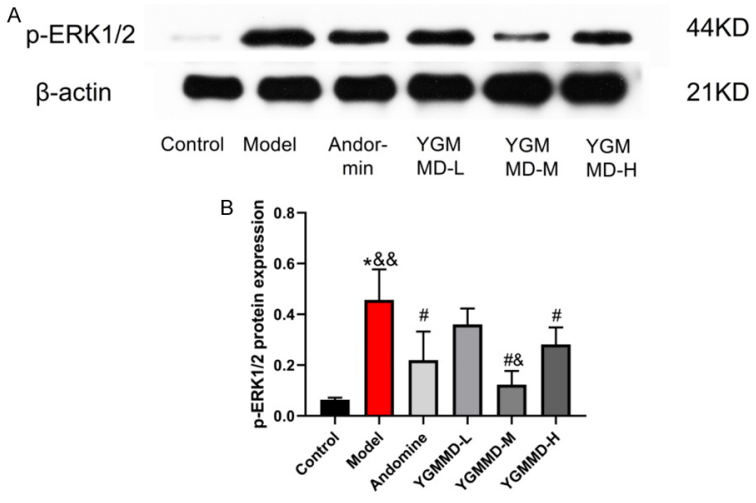

Figure 18. Expression of p-ERK1/2 protein in the retinal tissues of the rats in different groups. A: Western blots for p-ERK1/2; B: Quantitative analysis of expression levels of p-ERK1/2. *P < 0.05, vs. control; #P < 0.05, vs. Model; &P < 0.05, vs. Andomine.

can reduce the expression level of ERK [44-46]. Activation of the PI3K/Akt pathway can affect the expression of AQP4 and Kir4.1, and quercetin can directly inhibit the expression of AQP4 [47].

Further validation through *in vivo* experiments demonstrated that a moderate dose of YGMMD stabilized body weight and alleviated retinal edema and pathologic damage in SD rats. Additionally, immunohistochemistry, immunofluorescence, and protein blotting confirmed that the expression of AQP4 and ERK1/2 was elevated, whereas that of Kir4.1,

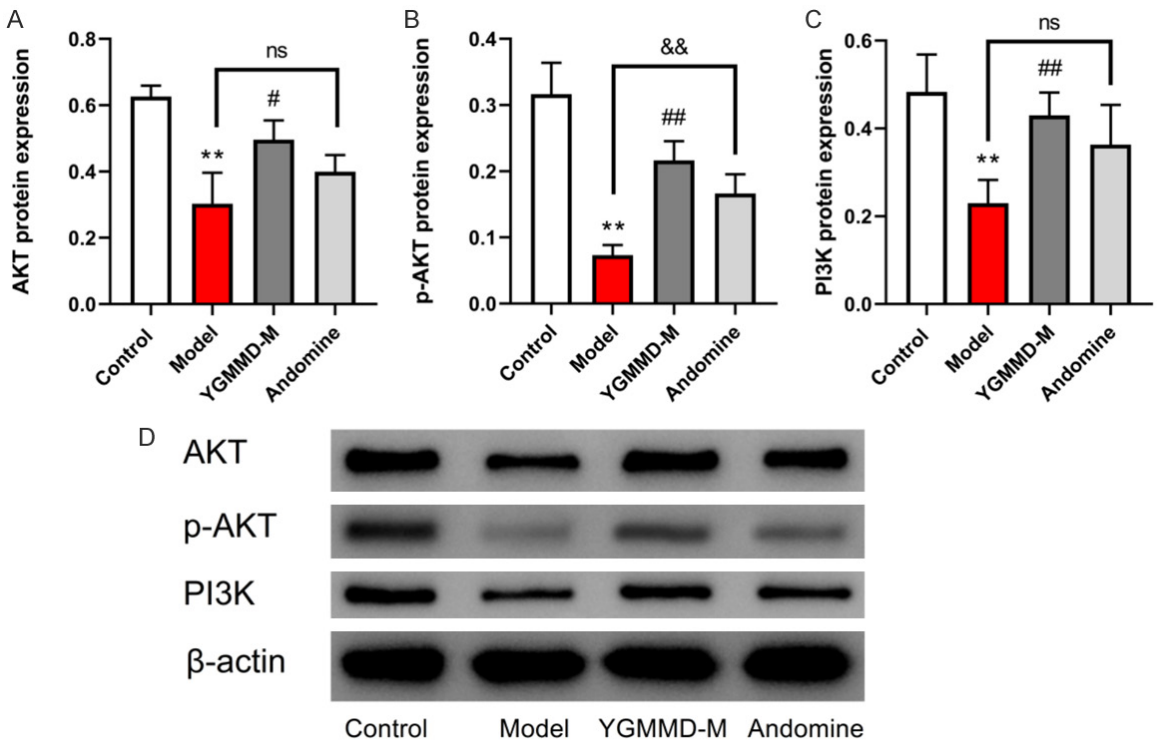

Figure 19. Expression of PI3K-AKT-related proteins in the retinal tissues of the rats in different groups. A: Quantitative analysis of expression levels of AKT; B: Quantitative analysis of expression levels of p-AKT; C: Quantitative analysis of expression levels of PI3K; D: Western blots for PI3K-AKT-related proteins. **P < 0.01, vs. Control; ##P < 0.01, vs. model; &&P < 0.01, vs. Andomine.

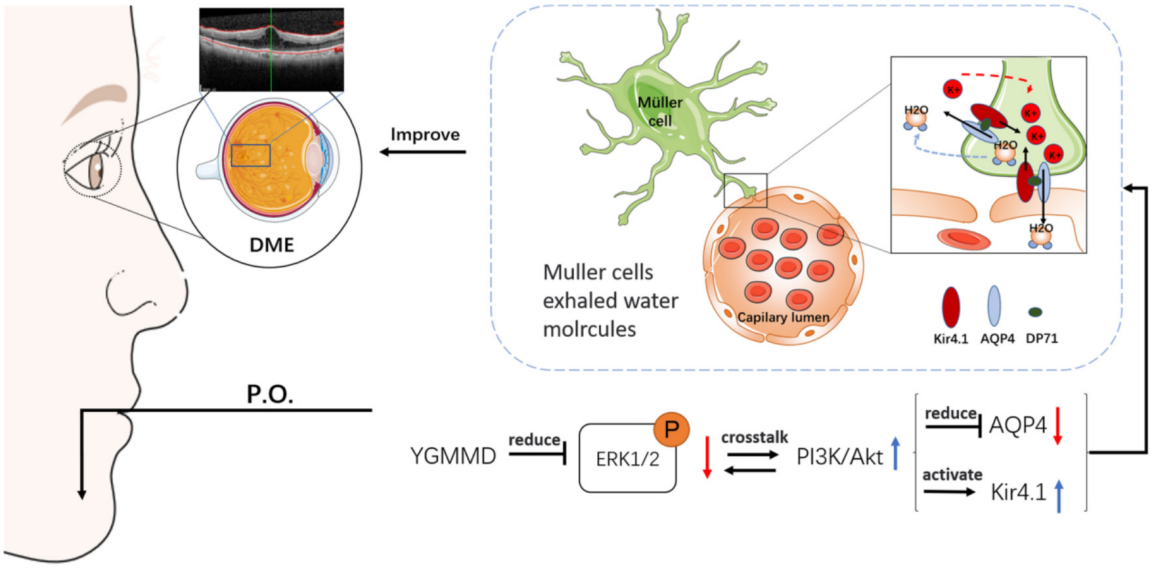

Figure 20. Possible mechanism of YGMMD in treating DME. It is speculated that YGMMD exerts its anti-DME effect by regulating AQP4/Kir4.1. YGMMD: Yigan Mingmu Decoction. DME: diabetic macular edema.

PI3K, and Akt was reduced in rats with diabetic retinal edema. However, treatment with YGMMD reversed these effects. These results indicate that YGMMD can prevent and treat DME by regulating AQP4 and Kir4.1, possibly through the ERK1/2/PI3K/AKT signaling path-

way. Furthermore, blood glucose monitoring revealed a significant decrease in blood glucose levels in the YGMMD-treated group, thereby improving DME. These findings also validate the reliability of network pharmacology research methods, implying that YGMMD may offer a breakthrough approach for treating DME through the downregulation of AQP4 and upregulation of Kir4.1.

This study had certain limitations. First, there was a lack of corresponding in vitro cell experiments to validate our findings. Second, genetic testing was not performed. Therefore, future studies should remedy these shortcomings.

Conclusion

Based on these experimental findings, it is plausible that YGMMD is possibly effective in the treatment of DME. This was achieved by suppressing the activation of p-ERK1/2 while simultaneously enhancing the expression of p-AKT, thereby reducing the levels of AQP4. Furthermore, YGMMD exhibited the potential to upregulate Kir4.1, which restores equilibrium in the retinal fluid clearance system. Consequently, this leads to improved absorption of retinal fluid and the alleviation of diabetic retinal edema. Moreover, YGMMD demonstrates its safety and efficacy by effectively lowering blood glucose levels, promoting weight management, mitigating Müller cell edema, and ameliorating pathological retinal damage in rats with diabetic retinal edema.

Acknowledgements

This work was supported by the Hunan Traditional Chinese Medicine Research Plan (C2022003), and Hunan University of Chinese Medicine Graduate Student Innovation Project (2022CX150, 2021CX16 and 2023CX39).

Disclosure of conflict of interest

None.

Address correspondence to: Xiangdong Chen, Department of Ophthalmology, The First Affiliated Hospital of Hunan University of Chinese Medicine, No. 95, Shaoshan Middle Road, Yuhua District, Changsha 431000, Hunan, China. Tel: +86-139-75866316; E-mail: 201602110134@stu.hnucm.edu.cn

References

[1] Schey KL, Wang Z, L Wenke J and Qi Y. Aquaporins in the eye: expression, function, and roles in ocular disease. Biochim Biophys Acta 2014; 1840: 1513-1523.

[2] Lisjak M, Potokar M, Zorec R and Jorgačevski J. Indirect role of AQP4b and AQP4d isoforms in dynamics of astrocyte volume and orthogonal arrays of particles. Cells 2020; 9: 735.

[3] Narayanan R and Kuppermann BD. Intracellular edema. Dev Ophthalmol 2017; 58: 21-26.

[4] Gallina D, Zelinka CP, Cebulla CM and Fischer AJ. Activation of glucocorticoid receptors in Muller glia is protective to retinal neurons and suppresses microglial reactivity. Exp Neurol 2015; 273: 114-125.

[5] Reed MM and Blazer-Yost B. Channels and transporters in astrocyte volume regulation in health and disease. Cell Physiol Biochem 2022; 56: 12-30.

[6] Midena E, Torresin T, Schiavon S, Danieli L, Polo C, Pilotto E, Midena G and Frizziero L. The disorganization of retinal inner layers is correlated to müller cells impairment in diabetic macular edema: an imaging and omics study. Int J Mol Sci 2023; 24: 9607.

[7] Beverley KM and Pattnaik BR. Inward rectifier potassium (Kir) channels in the retina: living our vision. Am J Physiol Cell Physiol 2022; 323: C772-C782.

[8] Du M, Li J, Chen L, Yu Y and Wu Y. Astrocytic Kir4.1 channels and gap junctions account for spontaneous epileptic seizure. PLoS Comput Biol 2018; 14: e1005877.

[9] Jiang YH, Li T, Liu Y, Liu X, Jia S, Hou C, Chen G, Wang H, Ling S, Gao Q, Wang XR and Wang YF. Contribution of inwardly rectifying K+ channel 4.1 of supraoptic astrocytes to the regulation of vasopressin neuronal activity by hypotonicity. Glia 2023; 71: 704-719.

[10] Zhou Z, Zhan J, Cai Q, Xu F, Chai R, Lam K, Luan Z, Zhou G, Tsang S, Kipp M, Han W, Zhang R and Yu ACH. The water transport system in astrocytes-aquaporins. Cells 2022; 11: 2564.

[11] Macaulay N. Molecular mechanisms of K+ clearance and extracellular space shrinkage-Glia cells as the stars. Glia 2020; 68: 2192-2211.

[12] Fujimoto T, Stam K, Yaoi T, Nakano K, Arai T, Okamura T and Itoh K. Dystrophin short product, Dp71, interacts with AQP4 and Kir4.1 channels in the mouse cerebellar glial cells in contrast to Dp427 at inhibitory postsynapses in the purkinje neurons. Mol Neurobiol 2023; 60: 3664-3677.

[13] Vujosevic S, Micera A, Bini S, Berton M, Esposito G and Midena E. Aqueous humor biomark-

ers of Müller cell activation in diabetic eyes. Invest Ophthalmol Vis Sci 2015; 56: 3913-3918.
[14] Chen XD, Qin GY, Zhang YW, Sun SM, Nie FJ and Peng QH. Self-designed Yigan Mingmu Decoction for treating cystoid macular edema: a case report. Hunan J Tradit Chin Med 2017; 33: 79-80.
[15] Wang X. Intervention mechanism of Yigan Mingmu Decoction on autophagy of Müller cells in diabetic retinopathy edema model of SD rats. Master's thesis, Hunan Univ Chin Med 2021.
[16] Lian YT, Liu ZM, Nie FJ, Hu ZY, Fu ML, Hu Q, Jiang JY and Chen XD. Effects of Yigan Mingmu Decoction on the NLRP3/Caspase-1 signaling pathway in diabetic retinopathy edema model rats. J Hunan Univ Chin Med 2023; 43: 421-429.
[17] Ru J, Li P, Wang J, Zhou W, Li B, Huang C, Li P, Guo Z, Tao W, Yang Y, Xu X, Li Y, Wang Y and Yang L. TCMSP: a database of systems pharmacology for drug discovery from herbal medicines. J Cheminform 2014; 6: 13.
[18] Breuza L, Poux S, Estreicher A, Famiglietti ML, Magrane M, Tognolli M, Bridge A, Baratin D and Redaschi N; UniProt Consortium. The UniProtKB guide to the human proteome. Database (Oxford) 2016; 2016: bav120.
[19] Safran M, Dalah I, Alexander J, Rosen N, Iny Stein T, Shmoish M, Nativ N, Bahir I, Doniger T, Krug H, Sirota-Madi A, Olender T, Golan Y, Stelzer G, Harel A and Lancet D. GeneCards Version 3: the human gene integrator. Database (Oxford) 2010; 2010: baq020.
[20] Amberger JS, Bocchini CA, Schiettecatte F, Scott AF and Hamosh A. OMIM.org: Online Mendelian Inheritance in Man (OMIM®), an online catalog of human genes and genetic disorders. Nucleic Acids Res 2015; 43: D789-D798.
[21] Huang XF, Zhang JL, Huang DP, Huang AS, Huang HT, Liu Q, Liu XH and Liao HL. A network pharmacology strategy to investigate the anti-inflammatory mechanism of luteolin combined with in vitro transcriptomics and proteomics. Int Immunopharmacol 2020; 86: 106727.
[22] Doncheva NT, Morris JH, Gorodkin J and Jensen LJ. Cytoscape StringApp: network analysis and visualization of proteomics data. J Proteome Res 2018; 18: 623-632.
[23] Trott O and Olson AJ. AutoDock Vina: improving the speed and accuracy of docking with a new scoring function, efficient optimization, and multithreading. J Comput Chem 2010; 31: 455-461.
[24] Zhou Y, Zhou B, Pache L, Chang M, Khodabakhshi AH, Tanaseichuk O, Benner C and Chanda SK. Metascape provides a biologist-oriented resource for the analysis of systems-level datasets. Nat Commun 2019; 10: 1523.
[25] Burley SK, Berman HM, Kleywegt GJ, Markley JL, Nakamura H and Velankar S. Protein Data Bank (PDB): the single global macromolecular structure archive. Methods Mol Biol 2017; 1607: 627-641.
[26] Seeliger D and De Groot BL. Ligand docking and binding site analysis with PyMOL and Autodock/Vina. J Comput Aided Mol Des 2010; 24: 417-422.
[27] Chen XD, Sun SM and Nie FJ. Establishment of streptozotocin-induced diabetic retinopathy model in Brown Norway rats. Chin J Tradit Chin Med Pharm 2018; 24: 15-19.
[28] Zudaire E, Gambardella L, Kurcz C and Vermeren S. A computational tool for quantitative analysis of vascular networks. PLoS One 2011; 6: e27385.
[29] Bordoni L, Thoren AE, Gutiérrez-Jiménez E, Åbjørsbråten KS, Bjørnstad DM, Tang W, Stern M, Østergaard L, Nagelhus EA, Frische S, Ottersen OP and Enger R. Deletion of aquaporin-4 improves capillary blood flow distribution in brain edema. Glia 2023; 71: 2559-2572.
[30] Netti V, Fernández J, Melamud L, Garcia-Miranda P, Di Giusto G, Ford P, Echevarría M and Capurro C. Aquaporin-4 removal from the plasma membrane of human müller cells by AQP4-IgG from patients with neuromyelitis optica induces changes in cell volume homeostasis: the first step of retinal injury. Mol Neurobiol 2021; 58: 5178-5193.
[31] Djukic B, Casper KB, Philpot BD, Chin LS and Mccarthy KD. Conditional knock-out of Kir4.1 leads to glial membrane depolarization, inhibition of potassium and glutamate uptake, and enhanced short-term synaptic potentiation. J Neurosci 2007; 27: 11354-11365.
[32] Fang XL, Zhang Q, Xue WW, Tao JH, Zou HD, Lin QR and Wang YL. Suppression of cAMP/PKA/CREB signaling ameliorates retinal injury in diabetic retinopathy. Kaohsiung J Med Sci 2023; 39: 916-926.
[33] Jiang YH, Li T, Liu Y, Liu X, Jia S, Hou C, Chen G, Wang H, Ling S, Gao Q, Wang XR and Wang YF. Contribution of inwardly rectifying K+ channel 4.1 of supraoptic astrocytes to the regulation of vasopressin neuronal activity by hypotonicity. Glia 2023; 71: 704-719.
[34] Elsherbini DMA, Ghoneim FM, El-Mancy EM, Ebrahim HA, El-Sherbiny M, El-Shafey M, Al-Serwi RH and Elsherbiny NM. Astrocytes profiling in acute hepatic encephalopathy: possible enrolling of glial fibrillary acidic protein, tumor necrosis factor-alpha, inwardly rectifying potassium channel (Kir 4.1) and aquaporin-4 in rat cerebral cortex. Front Cell Neurosci 2022; 16: 896172.
[35] Kim JE, Park H, Lee JE and Kang TC. Blockade of 67-kDa laminin receptor facilitates AQP4

down-regulation and BBB disruption via ERK1/2-and p38 MAPK-mediated PI3K/AKT activations. Cells 2020; 9: 1670.
[36] Tu Y, Zhu M, Wang Z, Wang K, Chen L, Liu W, Shi Q, Zhao Q, Sun Y, Wang X, Song E and Liu X. Melatonin inhibits Müller cell activation and pro-inflammatory cytokine production via up-regulating the MEG3/miR-204/Sirt1 axis in experimental diabetic retinopathy. J Cell Physiol 2020; 235: 8724-8735.
[37] Park H, Choi SH, Kong MJ and Kang TC. Dysfunction of 67-kDa laminin receptor disrupts BBB integrity via impaired dystrophin/AQP4 complex and p38 MAPK/VEGF activation following status epilepticus. Front Cell Neurosci 2019; 13: 236.
[38] Stulpinas A, Sereika M, Vitkeviciene A, Imbrasaite A, Krestnikova N and Kalvelyte AV. Crosstalk between protein kinases AKT and ERK1/2 in human lung tumor-derived cell models. Front Oncol 2023; 12: 1045521.
[39] Milton M and Smith PD. It's all about timing: the involvement of Kir4.1 channel regulation in acute ischemic stroke pathology. Front Cell Neurosci 2018; 12: 36.
[40] Zaika O, Palygin O, Tomilin V, Mamenko M, Staruschenko A and Pochynyuk O. Insulin and IGF-1 activate Kir4.1/5.1 channels in cortical collecting duct principal cells to control basolateral membrane voltage. Am J Physiol Renal Physiol 2016; 310: F311-F321.
[41] Yang L, Guo W, Zhang Q, Li H, Liu X, Yang Y, Zuo J and Liu W. Crosstalk between Raf/MEK/ERK and PI3K/AKT in suppression of Bax conformational change by Grp75 under glucose deprivation conditions. J Mol Biol 2011; 414: 654-666.
[42] Yu LN, Zhou XL, Yu J, Huang H, Jiang LS, Zhang FJ, Cao JL and Yan M. PI3K contributed to modulation of spinal nociceptive information related to ephrinBs/EphBs. PLoS One 2012; 7: e40930.
[43] Guan XH, Fu QC, Shi D, Bu HL, Song ZP, Xiong BR, Shu B, Xiang HB, Xu B, Manyande A, Cao F and Tian YK. Activation of spinal chemokine receptor CXCR3 mediates bone cancer pain through an Akt-ERK crosstalk pathway in rats. Exp Neurol 2015; 263: 39-49.
[44] Yang Y, Yan J, Huang J, Wu X, Yuan Y, Yuan Y, Zhang S and Mo F. Exploring the mechanism by which quercetin re-sensitizes breast cancer to paclitaxel: network pharmacology, molecular docking, and experimental verification. Naunyn Schmiedebergs Arch Pharmacol 2023; 396: 3045-3059.
[45] Ji X, Du W, Che W, Wang L and Zhao L. Apigenin inhibits the progression of osteoarthritis by mediating macrophage polarization. Molecules 2023; 28: 2915.
[46] Wang Z, Sun W, Sun X, Wang Y and Zhou M. Kaempferol ameliorates Cisplatin induced nephrotoxicity by modulating oxidative stress, inflammation and apoptosis via ERK and NF-κB pathways. AMB Express 2020; 10: 58.
[47] Kumar B, Gupta SK, Nag TC, Srivastava S, Saxena R, Jha KA and Srinivasan BP. Retinal neuroprotective effects of quercetin in streptozotocin-induced diabetic rats. Exp Eye Res 2014; 125: 193-202.